

ACCELERATOR, REACTOR, SOLAR AND ATMOSPHERIC NEUTRINO OSCILLATION: BEYOND THREE GENERATIONS

Srubabati Goswami
Department of Pure Physics,
University of Calcutta,
92 Acharya Prafulla Chandra Road,
Calcutta 700 009, INDIA.

P.A.C.S. Nos.: 14.60.Pq, 14.60.Lm, 96.40.Tv, 96.60 Kx

We perform a phenomenological analysis of neutrino oscillation in a four generation framework introducing an additional sterile neutrino. In such a scenario, more than one pattern is possible that can accommodate three hierarchically different mass squared differences as required by the present experiments. We considered two different spectrums. Choosing the Δm^2 s in the ranges suitable for the LSND, atmospheric and solar neutrino oscillation, limits on the mixing angles are derived, consistent with the most restrictive accelerator and reactor data as well as the atmospheric and solar neutrino results. The allowed mixing angles are found to be constrained very severely in both cases. For one mass pattern in the combined allowed zone the atmospheric anomaly can be explained by $\nu_e - \nu_\mu$ oscillation whereas for the other the $\nu_\mu - \nu_\tau$ channel is preferred. The accelerator experiments CHORUS and NOMAD have different sensitivities in these regions and they can distinguish between the two choices.

June 28, 1995

1 INTRODUCTION

The question whether neutrinos have a non-zero mass or not has remained one of the most tantalising issues in present day physics. In the standard model of electroweak theory the neutrinos are considered to be massless. But there is no compelling theoretical reason behind this assumption. Most extensions of the standard model allow small but non-zero neutrino mass. A way for probing small neutrino masses and the mixing between different neutrino flavours is provided by neutrino oscillations. Considering only two generations for simplicity, the probability that an initial ν_α of energy E gets converted to a ν_β after travelling a distance L in vacuum is

$$P_{\nu_\alpha\nu_\beta} = \sin^2 2\theta \sin^2(1.27\Delta m^2 L/E) \quad (1)$$

where θ is the mixing angle in vacuum. Δm^2 denotes the mass difference squared in eV^2 . L/E is in meter/MeV. The oscillatory character is embedded in the second factor in (1). The detection of this phenomenon in an experiment requires $E/L \simeq \Delta m^2$.

Recently the Liquid Scintillator Neutrino Detector (LSND) collaboration has declared its results for a positive evidence of $\bar{\nu}_\mu - \bar{\nu}_e$ oscillation [1]. Prior to this, indications of neutrino oscillations came from the well known solar neutrino problem and the atmospheric neutrino anomaly.

If indeed neutrino flavour oscillation takes place, the most sensitive value of Δm^2 for detecting such a phenomenon in LSND is $\sim 6eV^2$, which is in the right ballpark for the cold plus hot dark matter scenario for structure formation in the early universe [2]. It remains to be seen whether the LSND results stand the test of time but already this has added a new impetus to the issue of neutrino mass and mixing and a number of investigations have been carried out recently, discussing the possible impact of this on particle physics, astrophysics and cosmology [3, 4].

The observed suppression of the solar neutrino fluxes as compared to the theoretical predictions constitutes the long standing solar neutrino problem. A purely astrophysical solution to this, attributing the deficit to an inaccurate prediction of the fluxes by the standard solar models [5] is disfavoured by the present data [6]. If neutrinos are massive, a plausible explanation to the solar neutrino problem is neutrino oscillation in vacuum [7] or the Mikheyev-Smirnov-Wolfenstein (MSW) [8] effect of matter enhanced oscillations. The basic idea is flavour conversion of ν_e to another species – active or sterile – to which the detector is not sensitive. The two generation oscillation explanation for the solar neutrino problem requires $\Delta m^2 \sim 6 \times 10^{-6} eV^2$ and $\sin^2 2\theta \sim 7 \times 10^{-3}$ (non-adiabatic solution) and $\Delta m^2 \sim 9 \times 10^{-6} eV^2$ and $\sin^2 2\theta \sim 0.6$ (large mixing angle solution) [9] for the MSW matter oscillation to an active neutrino. If instead one considers oscillation to sterile neutrinos as a possible solution, the large angle region is excluded at 99% C.L. [9]. This region is also not consistent with the bound on the number of neutrino species in big-bang nucleosynthesis [10]. Oscillation in vacuum to an active neutrino requires $\Delta m^2 \sim (0.45 - 1.2) \times 10^{-10} eV^2$ and

$\sin^2 2\theta \sim (0.6 - 1.0)$ [11]. The sterile neutrino alternative for this case is ruled out by the present data at 98% C.L [12].

The primary components of the cosmic-ray flux interact with the earth's atmosphere producing pions and kaons which can decay as:

$$\begin{aligned}\pi^+(K^\pm) &\rightarrow \mu^\pm + \nu_\mu(\bar{\nu}_\mu) \\ \mu^\pm &\rightarrow e^\pm + \nu_e(\bar{\nu}_e) + \bar{\nu}_\mu(\nu_\mu)\end{aligned}$$

These neutrinos can be detected by imaging water Čerenkov detectors, – Kamiokande [13, 14] and IMB [15] – or using iron calorimeters as is done in Fréjus [16], Nusex [17] and Soudan2 [18]. To reduce the uncertainty in the absolute flux values the usual practice is to present the ratio of ratios R [19] :

$$R = \frac{(\nu_\mu + \bar{\nu}_\mu)/(\nu_e + \bar{\nu}_e)_{\text{obsvd}}}{(\nu_\mu + \bar{\nu}_\mu)/(\nu_e + \bar{\nu}_e)_{\text{MC}}} \quad (2)$$

where MC denotes the Monte-Carlo simulated ratio. Kamiokande and IMB find R to be less than the expected value of unity. This deviation is known as the atmospheric neutrino anomaly. The preliminary results from Soudan2 agrees with this but Fréjus and Nusex do not support this conclusion. The atmospheric anomaly, if it exists, can be explained by either $\nu_\mu - \nu_e$ or $\nu_\mu - \nu_\tau$ oscillations in a two generation picture. The analysis of the new multi-GeV data as well as the previous sub-GeV data of the Kamiokande collaboration predicts the following best-fit parameters $(\Delta m^2, \sin^2 2\theta) = (1.8 \times 10^{-2} eV^2, 1.0)$ for $\nu_\mu - \nu_e$ oscillation and $(1.6 \times 10^{-2} eV^2, 1.0)$ for $\nu_\mu - \nu_\tau$ oscillation [14]. Since the required mixing angle is large, oscillation to sterile neutrinos is again inconsistent with the nucleosynthesis constraints [10].

The three neutrino oscillation phenomena mentioned above – namely the solar neutrino problem, the atmospheric neutrino anomaly and the $\bar{\nu}_\mu - \bar{\nu}_e$ oscillations observed by LSND group – require three hierarchically different mass ranges and a simultaneous explanation of all of them would need at least four generations of neutrinos [3]. LEP data reveals that there are three light active neutrino species. This is supported by the requirements of nucleosynthesis in the early universe. So the fourth neutrino has to be sterile. Introducing this new neutrino one can attempt separate two generation treatments for each but a more comprehensive approach would be to determine the parameter ranges consistent with all the experiments by a combined four generation analysis which can reveal the full implications of each experimental data on the other. In this paper we perform such an oscillation analysis in a four family picture.

In a four generation scenario there are six Δm^2 s, three of which are independent and six mixing angles neglecting the CP violating phases. We assume a minimal four flavour mixing scheme, in which the sterile neutrino mixes only with the electron neutrino, thus reducing the number of mixing angles to four. We do not make any

assumptions regarding these mixing angles allowing them to cover the whole range from 0 to $\pi/2$. Guided by the present data on neutrino oscillation we consider two different sets of hierarchical mass squared differences:

(i) $\Delta_{13} \simeq \Delta_{23} \simeq \Delta_{34} = \Delta_{LSND}$ in the LSND range,
 $\Delta_{12} \simeq \Delta_{24} = \Delta_{ATM}$ as preferred by the atmospheric neutrino data and
 $\Delta_{14} = \Delta_{SOLAR}$ either in the MSW or in the vacuum oscillation range.

(ii) $\Delta_{12} \simeq \Delta_{13} \simeq \Delta_{24} \simeq \Delta_{34} = \Delta_{LSND}$

$\Delta_{23} = \Delta_{ATM}$

$\Delta_{14} = \Delta_{SOLAR}$

$\Delta_{ij} = |m_j^2 - m_i^2|$. The hierarchy in the absolute values of neutrino masses as implied by the above spectrums can be classified in general as

Case (i) : (a) $m_1^2 \simeq m_4^2 \ll m_2^2 \approx m_3^2$ or (b) $m_1^2 \simeq m_4^2 \gg m_2^2 \approx m_3^2$

Case (ii): (a) $m_1^2 \simeq m_4^2 \approx m_2^2 \ll m_3^2$ or (b) $m_1^2 \simeq m_4^2 \approx m_2^2 \gg m_3^2$

These are shown schematically in fig. 1. The \simeq and \approx signs imply, differences by Δ_{SOLAR} and Δ_{ATM} are neglected respectively, while the \gg or \ll sign means difference by Δ_{LSND} . Neutrino oscillation analysis remains the same for types (a) and (b) in both cases and one has to invoke some other experimental constraints like that obtained from neutrinoless double beta decay for a distinction between these [20].

Models for neutrino masses and mixings assuming the existence of sterile states besides the three active flavours have been discussed before [21]. After the declaration of the LSND results models involving extra singlet neutrinos have been constructed by many authors [22]. Our investigation is not motivated by any particular model. Rather, we do a phenomenological analysis fixing the Δm^2 's in the ranges suitable for explaining the solar neutrino, atmospheric neutrino and the LSND results and determine the allowed values of the mixing angles, which can reconcile all the experimental data. The perspectives of the accelerator experiments CHORUS and NOMAD, searching for $\nu_\mu - \nu_\tau$ oscillations, are discussed in the light of our findings.

The plan of the paper is as follows. In section 2 we summarize the experimental results relevant for our purpose. In the following section the general multi-generation formalism for studying neutrino oscillations is developed. In Section 4 we calculate the survival and transition probabilities for the various experiments for the mass patterns (i) and (ii). The results of our analysis and some discussions are presented in section 5. We end in section 6 with a short summary and conclusions.

2 Experimental Results

2.1 Laboratory experiments

The laboratory experiments can serve as an important tool for neutrino oscillation search. These are either accelerator or reactor based and in general are of two types:

(i) Disappearance experiments: in which one looks for a reduction in the initial neutrino

flux due to oscillation to some other flavour to which the detector is not sensitive.

(ii) Appearance experiments: in which one searches for a new neutrino flavour, absent in the initial beam, which can arise from oscillation.

Prior to the LSND results all the laboratory experiments were consistent with no neutrino oscillations [23] and provided exclusion regions in the $\Delta m^2 - \sin^2 2\theta$ plane. In the region of large Δm^2 , the $\sin^2(1.27\Delta m^2 L/E)$ term $\rightarrow 0.5$ and $P_{\nu_\alpha\nu_\beta} = 0.5 \sin^2 2\theta$. Thus the limits on $\sin^2 2\theta$ from the exclusion plots can be used to provide bounds on $P_{\nu_\alpha\nu_\beta}$. Below we summarize the laboratory experiments which give most stringent bounds on $P_{\nu_\alpha\nu_\beta}$.

The reactor experiments are suitable for a search of $P_{\bar{\nu}_e\bar{\nu}_e}$ using disappearance technique. The most stringent constraint is provided by Bugey which measures the spectrum of $\bar{\nu}_e$, coming from the Pressurized Water Reactors running at the Bugey nuclear power plant, at 15, 40, and 95 metre using neutron detection techniques. The 90% C.L. exclusion contour implies $1 - P_{\bar{\nu}_e\bar{\nu}_e} \lesssim 0.05$ [24].

Accelerators produce mainly ν_μ beams – the ν_e component being small and poorly determined. The most restrictive accelerator based disappearance experiment measuring $P_{\bar{\nu}_\mu\bar{\nu}_\mu}$ is CDHSW. The 90% C.L. bound one obtains from the exclusion plot presented by the CDHSW collaboration is $P_{\nu_\mu\nu_\mu} \gtrsim 0.95$ [25].

Accelerator based appearance experiments searching for $\bar{\nu}_\mu \rightarrow \bar{\nu}_e$ oscillations are LSND, KARMEN and E776 at BNL. The last two experiments are consistent with no neutrino oscillation. KARMEN has so far quoted an upper limit on the oscillation probability as $P_{\bar{\nu}_\mu\bar{\nu}_e} \leq 3.1 \times 10^{-3}$ (90% C.L.) [26] whereas from the two flavour exclusion areas presented by BNL one gets $P_{\bar{\nu}_\mu\bar{\nu}_e} \lesssim 1.5 \times 10^{-3}$ (90% C.L.) [27] which is the more restrictive of the two. LSND has claimed a positive evidence for neutrino oscillations and reports an excess of $16.4^{+9.7}_{-8.9} \pm 3.3$ events over the estimated background which, if interpreted in terms of neutrino oscillations, corresponds to a probability $P_{\bar{\nu}_\mu\bar{\nu}_e}$ of $(0.34^{+0.20}_{-0.18} \pm 0.07)\%$ [1].

E531 at Fermilab looks for $\nu_\mu - \nu_\tau$ oscillation, by ν_τ appearance. Their results can be translated into an upper limit on the oscillation probability: $P_{\nu_\mu\nu_\tau} \lesssim 2 \times 10^{-3}$ [28].

CHORUS [29] and NOMAD [30] at CERN search for $\nu_\mu - \nu_\tau$ oscillation. With the CERN SPS designed to deliver 2.4×10^{19} protons, CHORUS and NOMAD are sensitive to a minimum oscillation probability of 10^{-4} .

These experiments are sensitive to different Δm^2 , because the L/E factor is different for each. In Table 1 we summarize the characteristics of the experiments which are most constraining and of CHORUS and NOMAD whose results are awaited.

2.2 Atmospheric neutrinos

Among the experiments measuring the atmospheric neutrino flux, data of most statistical significance have been collected by the Kamiokande and the IMB collaborations. For neutrinos of energy less than ~ 1 GeV, IMB finds $R = 0.54 \pm 0.05 \pm 0.12$ [15] in agreement with the Kamiokande data $R = 0.60^{+0.06}_{-0.05} \pm 0.05$ in this energy range [13, 14]. Recently the Kamiokande group has published the results of the measurement of the flux ratio in the multi-GeV energy range [14]. They found $R = 0.57^{+0.08}_{-0.07} \pm 0.07$ in good agreement with the sub-GeV value. Another aspect of this measurement that can independently point towards neutrino oscillation is the dependence of R on the zenith-angle. The multi-GeV Kamiokande data reveals a dependence on the zenith-angle unlike the sub-GeV data, though the statistical significance of this result has been questioned [31]. For the purpose of this paper we use the sub-GeV Kamiokande results.

2.3 Solar neutrinos

At present there are four ongoing experiments that are measuring the flux of solar neutrinos; the Homestake ^{37}Cl neutrino capture experiment, the Kamiokande ν -e scattering experiment and the ^{71}Ga neutrino capture experiments of the SAGE as well as the GALLEX collaborations. The measured rate for the chlorine experiment [32] is 2.55 ± 0.17 (stat) ± 0.18 (syst) SNU as compared to the standard model [33] prediction : $9.3^{+1.3}_{-1.4}$ SNU including metal and helium diffusion and $7.0^{+0.9}_{-1.0}$ SNU without any diffusion. The observed rates in the Ga experiments GALLEX [34] and SAGE [35] are respectively 79 ± 10 (stat) ± 6 (syst) SNU and 69 ± 11 (stat) $^{+5}_{-7}$ (syst) SNU while the theoretical prediction is 137^{+6}_{-7} SNU including diffusion and 126^{+6}_{-6} SNU for no diffusion. The measured flux in Kamiokande [36] is $[3.0 \pm 0.41$ (stat) ± 0.35 (syst)] $\times 10^{-6} \text{ cm}^{-2}\text{s}^{-1}$. This is 0.45 of the theoretical predictions including diffusion and 0.61 of the standard model rate without diffusion [33]. Thus all the experiments indicate deviations from the standard model predictions. The degree of depletion differ from experiment to experiment. Since each type of experiment is sensitive to different parts of the solar neutrino energy spectrum, it is plausible that the suppression mechanism is energy dependent. It has remained an unsettled issue for a long time and new experiments [37] are being set up to examine it from various angles.

3 Neutrino Oscillation

3.1 Vacuum Oscillation

If the neutrinos are massive then quark mixing suggests a leptonic mixing matrix analogous to the CKM matrix. Then, the flavour eigenstates, *i.e.* the states produced

in weak interaction decays are not the same as the mass eigenstates (which are the neutrino states that propagate) but linear combinations of them.

$$\nu_\alpha = \sum_{i=1}^N U_{\alpha i} \nu_i \quad (3)$$

U is the unitary mixing matrix. This leads to the possibility of neutrino oscillations. For N neutrino generations the expression (1) generalises to

$$P_{\nu_\alpha \nu_\beta} = \delta_{\alpha\beta} - 4 \sum_{j>i} U_{\alpha i} U_{\beta i} U_{\alpha j} U_{\beta j} \sin^2\left(\frac{\pi L}{\lambda_{ij}}\right) \quad (4)$$

i, j varies from 1 to N for N generations. $\lambda_{ij} = 2.47m(E_\nu/MeV)(eV^2/\Delta_{ij})$. The actual form of the various survival and transition probabilities will depend on the spectrum of Δm^2 chosen and the explicit form of U .

If Δm^2 is such that a particular $\lambda \gg L$, then the corresponding oscillatory term $\sin^2 \pi L/\lambda \rightarrow 0$, whereas $\lambda \ll L$ would imply a large number of oscillations and consequently the $\sin^2 \pi L/\lambda$ term averages out to $1/2$.

Since CP violating phases are discarded, U is real and in the minimal mixing scheme, is a function of four angles. One can express it in general as the product of four 4×4 rotation matrices, R_{ij} . The order in which the multiplication is to be performed is arbitrary leading to several different forms of U . In the quark sector considerable effort has been devoted to specify what would be a ‘good choice’ for $N=3$ as well as $N > 3$ [38]. All choices being mathematically equivalent, a good choice is mostly a matter of convenience, depending on how directly one can connect the experimentally determined quantities with the mixing angles. In the neutrino sector the experiments measure the energy and detector cross-section averaged survival or transition probabilities. Consequently a judicious choice of U in this case would be that in which one can minimise the number of mixing angles appearing in the various survival and transition probabilities. With this as the guideline for determining the mixing matrix U , we observe that the order in which the product of the rotation matrices are to be taken depends on the Δ_{ij} s chosen. As a general principle we fix the following rule: the rotations are to be performed in the order of increasing mass hierarchies. This is true even for a three generation analysis. As a consequence of CPT and CP invariance there is no distinction between $P_{\nu_\alpha \nu_\beta}, P_{\bar{\nu}_\alpha \bar{\nu}_\beta}, P_{\nu_\beta \nu_\alpha}, P_{\bar{\nu}_\beta \bar{\nu}_\alpha}$ in our analysis.

3.2 Matter Oscillation

The discussion on matter oscillations is geared towards the solar neutrino problem since we neglect the matter effects for the atmospheric neutrinos. For the mass scales involved in our analysis this is a good approximation [39].

We have kept Δ_{14} in the range suitable for solving the solar neutrino problem for both the mass patterns, implying $\nu_e - \nu_s$ oscillation as the dominant mode for depletion

of solar neutrinos. In a combined analysis, mixing of ν_e with ν_μ and ν_τ is also expected to affect the probabilities.

Solving the neutrino propagation equations in matter for more than two generations and arbitrary values of neutrino masses is in general a non-trivial exercise. MSW analysis for three neutrino generations and the conditions under which it simplifies have been studied by many authors [40]. A particularly simplifying assumption is one in which the problem reduces to an effective two generation case [41, 42]. Oscillation to sterile neutrinos as a solution to the solar neutrino problem has been pursued by many authors in a two generation framework – for both vacuum [43], and matter oscillations [44]. In the presence of more than two generations the propagation equations in matter differ from the two generation $\nu_e - \nu_s$ case, due to the charged current interactions of only ν_e with matter as well as the different neutral current interactions of the three active flavours and ν_s . In our analysis we follow the notations of [41] but extend it for four generations including the changes in the effective potentials arising from the presence of sterile neutrinos.

The neutrino propagation equation in matter for four neutrino generations is,

$$i \frac{d}{dx} \begin{pmatrix} \nu_e \\ \nu_\mu \\ \nu_\tau \\ \nu_x \end{pmatrix} = \frac{1}{2E} M_F^2 \begin{pmatrix} \nu_e \\ \nu_\mu \\ \nu_\tau \\ \nu_x \end{pmatrix} \quad (5)$$

where, the mass matrix M_F^2 in flavour basis is

$$M_F^2 = U M_D^2 U^\dagger + M_A^2 \quad (6)$$

$$M_D^2 = \begin{pmatrix} 0 & 0 & 0 & 0 \\ 0 & \Delta_{21} & 0 & 0 \\ 0 & 0 & \Delta_{31} & 0 \\ 0 & 0 & 0 & \Delta_{14} \end{pmatrix} + m_1^2 \mathbf{I} \quad (7)$$

$$M_A^2 = \begin{pmatrix} A_1 & 0 & 0 & 0 \\ 0 & 0 & 0 & 0 \\ 0 & 0 & 0 & 0 \\ 0 & 0 & 0 & A_2 \end{pmatrix} - A_2 \mathbf{I} \quad (8)$$

$A_1 = 2\sqrt{2}G_F n_e E$ and arises from the charged current interaction of ν_e with electrons while $A_2 = \sqrt{2}G_F n_n E$ is due to the neutral current interaction of ν_e, ν_μ as well as ν_τ with the neutrons. G_F is the Fermi coupling constant. n_e and n_n are the ambient electron and neutron density respectively. E is the neutrino energy. For $\Delta_{12}, \Delta_{13} \gg A_1$, M_F^2 can be separated into a 2×2 neutrino submatrix exactly of the two generation form and two decoupled neutrinos. Under these conditions MSW resonance occurs between the first and the fourth generation while the second and the third generation remain unaffected by matter. This conclusion has been checked in [41] for one mass squared

difference in the atmospheric range. Since $\Delta_{LSND} \gg \Delta_{ATM}$, the above argument is expected to be valid for this mass scale also. We evaluate the survival probabilities in this approximation in the subsequent section for both the mass patterns.

4 Survival and Transition Probabilities

The oscillations are characterised by three oscillation wavelengths λ_{LSND} , λ_{ATM} , λ_{SOLAR} corresponding to the three mass scales, Δ_{LSND} , Δ_{ATM} and Δ_{SOLAR} in the problem. We note the following general points:

(i) Accelerator and Reactor Neutrinos

For the accelerator and reactor neutrinos, the energy and length scales are such that λ_{SOLAR} and $\lambda_{ATM} \gg L$ (see Table 1) and the oscillations driven by these mass scales are absent. Thus the one mass scale dominance often used in the context of accelerator and reactor neutrino oscillation [42, 45] is a valid approximation, the oscillations being driven by λ_{LSND} . We further note that for Bugey $\lambda_{LSND} \ll L$ so that $\sin^2(\pi L/\lambda_{LSND})$ averages to 1/2.

(ii) Atmospheric neutrinos

For the atmospheric neutrinos in the energy range $\sim (0.1 - 1)$ GeV travelling through a distance ranging from $\sim (10 - 10^4)$ km, $\lambda_{LSND} \ll L$ and $\sin^2(\pi L/\lambda_{LSND})$ can be replaced by the average value 1/2. On the other hand $\lambda_{SOLAR} \gg L$ and the oscillations driven by the mass scale relevant for the solar neutrino problem vanish in this case.

(iii) Solar neutrinos

For oscillation of solar neutrinos in vacuum λ_{LSND} and $\lambda_{ATM} \ll L$ and the terms involving these average out to 1/2.

4.1 Mass Spectrum (i)

Following the prescription described in section 3.1,

$$\begin{aligned}
 U &= R_{23}R_{13}R_{12}R_{14} \\
 &= \begin{pmatrix} c_{12}c_{13}c_{14} & s_{12}c_{13} & s_{13} & c_{13}c_{12}s_{14} \\ -c_{23}s_{12}c_{14} - s_{13}c_{12}s_{23}c_{14} & c_{12}c_{23} - s_{13}s_{12}s_{23} & s_{23}c_{13} & -c_{23}s_{12}s_{14} - s_{13}c_{12}s_{23}s_{14} \\ s_{12}s_{23}c_{14} - s_{13}c_{12}c_{23}c_{14} & -c_{12}s_{23} - s_{13}s_{12}c_{23} & c_{13}c_{23} & s_{12}s_{23}s_{14} - s_{13}c_{12}c_{23}s_{14} \\ -s_{14} & 0 & 0 & c_{14} \end{pmatrix} \quad (9)
 \end{aligned}$$

where $c_{ij} = \cos \theta_{ij}$ and $s_{ij} = \sin \theta_{ij}$, here and everywhere else in the paper. Let us now see what the probabilities for the various experiments are in this case.

(i) Accelerator and Reactor Experiments

$$P_{\bar{\nu}_e \bar{\nu}_e} = 1 - 2s_{13}^2 c_{13}^2 \quad (Bugey) \quad (10)$$

$$P_{\bar{\nu}_\mu \bar{\nu}_\mu} = 1 - 4s_{23}^2 c_{13}^2 (1 - c_{13}^2 s_{23}^2) \sin^2(\pi L / \lambda_{LSND}) \quad (CDHSW) \quad (11)$$

$$P_{\bar{\nu}_\mu \bar{\nu}_e} = 4c_{13}^2 s_{13}^2 s_{23}^2 \sin^2(\pi L / \lambda_{LSND}) \quad (LSND, E776) \quad (12)$$

$$P_{\bar{\nu}_\mu \bar{\nu}_\tau} = 4c_{23}^2 s_{23}^2 c_{13}^4 \sin^2(\pi L / \lambda_{LSND}) \quad (E531, CHORUS, NOMAD) \quad (13)$$

(ii) Atmospheric neutrinos

The general expression of (2) for N flavours in terms of the neutrino transition and survival probabilities is

$$R = \frac{P_{\nu_\mu \nu_\mu} + r_{MC} P_{\nu_\mu \nu_e}}{P_{\nu_e \nu_e} + \frac{1}{r_{MC}} P_{\nu_\mu \nu_e}} \quad (14)$$

where $r_{MC} = (\nu_e + \bar{\nu}_e) / (\nu_\mu + \bar{\nu}_\mu)$ as obtained from a Monte-Carlo simulation. In this case the relevant probabilities appearing in (14) are

$$P_{\nu_e \nu_e} = 1 - 2c_{13}^2 s_{13}^2 - 4c_{12}^2 s_{12}^2 c_{13}^4 \sin^2(\pi L / \lambda_{ATM}) \quad (15)$$

$$P_{\nu_\mu \nu_e} = 2c_{13}^2 s_{13}^2 s_{23}^2 + 4c_{13}^2 c_{12} s_{12} (c_{23} c_{12} - s_{13} s_{12} s_{23}) (c_{23} s_{12} + s_{13} c_{12} s_{23}) \sin^2(\pi L / \lambda_{ATM}) \quad (16)$$

$$P_{\nu_\mu \nu_\mu} = 1 - 2c_{13}^2 s_{23}^2 + 2c_{13}^4 s_{23}^4 - 4 \sin^2(\pi L / \lambda_{ATM}) (c_{23} c_{12} - s_{13} s_{12} s_{23})^2 (c_{23} s_{12} + s_{13} c_{12} s_{23})^2 \quad (17)$$

(iii) Solar neutrinos

(a) Vacuum Oscillations

The electron neutrino survival probability in this case is,

$$P_{\nu_e \nu_e} = c_{13}^4 c_{12}^4 P_{2VAC} + s_{13}^4 + s_{12}^4 c_{13}^4 \quad (18)$$

where P_{2VAC} is of the form of the two generation vacuum oscillation probability:

$$P_{2VAC} = 1 - \sin^2 2\theta_{14} \sin^2(\pi L / \lambda_{SOLAR}) \quad (19)$$

(b) MSW oscillations

If the mass hierarchies, mixing angles and the density distributions are such that one has resonance between the first and the fourth mass eigenstates, while the second and the third mass eigenstates remain independent of matter density then the mixing matrix in matter is $U_M = R_{23} R_{13} R_{12} R_{14M}$. The mixing between the first and the fourth generation gets modified by the matter effects as,

$$\tan 2\theta_{14m} = \frac{\Delta_{14} \sin 2\theta_{14}}{\Delta_{14} \cos 2\theta_{14} - 2\sqrt{2} G_F n_{eff} E} \quad (20)$$

where we define n_{eff} as

$$n_{eff} = c_{13}^2 c_{12}^2 n_e - \frac{1}{2} n_n \quad (21)$$

In the limit $c_{13}, c_{12} \rightarrow 1$ this reduces to the two generation limit for oscillation between ν_e and ν_s [44]. From (20), the resonance condition between the first and the fourth generation in the presence of the other two generations becomes

$$2\sqrt{2}G_F n_{eff} E = \Delta_{14} \cos 2\theta_{14} \quad (22)$$

The difference of this with the three generation resonance is to be noted. While the three generation resonance condition gets modified by one additional mixing angle here the mixing angles with the second as well as the third generation appear in the resonance condition through n_{eff} . The calculation of the survival probability $P_{\nu_e \nu_e}$ is then a straight-forward generalisation of the standard two or three generation MSW scenario and one gets,

$$P_{\nu_e \nu_e} = c_{12}^4 c_{13}^4 P_{MSW} + s_{13}^4 + s_{12}^4 c_{13}^4 \quad (23)$$

$$P_{MSW} = 0.5 + (0.5 - \theta(E - E_A)X) \cos 2\theta_{14} \cos 2\theta_{14M} \quad (24)$$

$E_A = \Delta_{14} \cos 2\theta_{14} / 2\sqrt{2}G_F n_{eff}$ gives the minimum ν energy that can encounter a resonance inside the sun. For this case the jump probability X , between the first and the fourth mass eigenstates, as obtained in the Landau-Zener approximation is

$$X = \exp \left(-\pi \Delta_{14} \sin^2 2\theta_{14} / 4E \cos 2\theta_{14} \frac{1}{n_{eff}} \left(\frac{dn_{eff}}{dx} \right)_{res} \right) \quad (25)$$

We note that unlike the case discussed in [41], the mixing angles c_{12}^2, c_{13}^2 appear in the expression of the jump probability, via n_{eff} defined in (21).

4.2 Mass Spectrum (ii)

This case has been considered also in [46], following slightly different notations. We discuss this to make the paper self contained and to facilitate the comparison between the results obtained for the two mass patterns. Following the rule we specified U in this case is

$$\begin{aligned} U &= R_{13} R_{12} R_{23} R_{14} \\ &= \begin{pmatrix} c_{12} c_{13} c_{14} & s_{12} c_{13} c_{23} - s_{13} s_{23} & c_{13} s_{12} s_{23} + s_{13} c_{23} & c_{13} c_{12} s_{14} \\ -s_{12} c_{14} & c_{12} c_{23} & c_{12} s_{23} & -s_{12} s_{14} \\ -s_{13} c_{12} s_{14} & -s_{13} s_{12} c_{23} - c_{13} s_{23} & -s_{12} s_{13} s_{23} + c_{13} c_{23} & -s_{13} c_{12} s_{14} \\ -s_{14} & 0 & 0 & c_{14} \end{pmatrix} \quad (26) \end{aligned}$$

This reduces to the three generation case discussed in [47] in the limit of θ_{14} going to zero. We next calculate the probabilities explicitly for the various experiments.

(i) Accelerator and Reactor Experiments

$$P_{\bar{\nu}_e \bar{\nu}_e} = 1 - 2c_{13}^2 c_{12}^2 + 2c_{13}^4 c_{12}^4 \quad (Bugey) \quad (27)$$

$$P_{\bar{\nu}_\mu \bar{\nu}_\mu} = 1 - \sin^2 2\theta_{12} \sin^2(\pi L/\lambda_{LSND}) \quad (CDHSW) \quad (28)$$

$$P_{\bar{\nu}_\mu \bar{\nu}_e} = 4c_{12}^2 s_{12}^2 c_{13}^2 \sin^2(\pi L/\lambda_{LSND}) \quad (LSND, E776) \quad (29)$$

$$P_{\bar{\nu}_\mu \bar{\nu}_\tau} = 4c_{12}^2 s_{12}^2 s_{13}^2 \sin^2(\pi L/\lambda_{LSND}) \quad (E531, CHORUS, NOMAD) \quad (30)$$

(ii) Atmospheric neutrinos

For the chosen mass pattern and mixing the probabilities appearing in (14) are

$$P_{\nu_e \nu_e} = 1 - 2c_{13}^2 c_{12}^2 + 2c_{13}^4 c_{12}^4 - 4(c_{13}s_{12}c_{23} - s_{13}s_{23})^2 (c_{13}s_{12}s_{23} + s_{13}c_{23})^2 \sin^2(\pi L/\lambda_{ATM}) \quad (31)$$

$$P_{\nu_\mu \nu_e} = 2c_{13}^2 c_{12}^2 s_{12}^2 - 4c_{12}^2 c_{23}s_{23}(c_{13}s_{12}c_{23} - s_{13}s_{23})(c_{13}s_{12}s_{23} + s_{13}c_{23}) \sin^2(\pi L/\lambda_{ATM}) \quad (32)$$

$$P_{\nu_\mu \nu_\mu} = 1 - 2c_{12}^2 s_{12}^2 - 4c_{12}^4 c_{23}^2 s_{23}^2 \sin^2(\pi L/\lambda_{ATM}) \quad (33)$$

(iii) Solar neutrinos

(a) Vacuum Oscillations

The electron neutrino survival probability in this case is,

$$P_{\nu_e \nu_e} = c_{13}^4 c_{12}^4 P_{2VAC} + (s_{12}c_{13}c_{23} - s_{13}s_{23})^4 + (c_{13}s_{12}s_{23} + s_{13}c_{23})^4 \quad (34)$$

where P_{2VAC} is given by eqn. (19).

(b) MSW oscillations

In this case the mixing matrix in matter is, $U_M = R_{13}R_{12}R_{23}R_{14M}$. For this also the resonance can be assumed to happen between the first and the fourth mass eigenstates whence the mixing angle θ_{14M} and the resonance condition continue to be given by eqns. (20) and (22). The probability however is different and can be expressed as,

$$P_{\nu_e \nu_e} = c_{12}^4 c_{13}^4 P_{MSW} + (s_{12}c_{13}c_{23} - s_{13}s_{23})^4 + (c_{13}s_{12}s_{23} + s_{13}c_{23})^4 \quad (35)$$

where P_{MSW} is defined in eqn. (24).

5 Results and Discussions

For both the mass spectrums discussed in sections 4.1 and 4.2, the survival or transition probabilities for the accelerator and reactor experiments are functions of any two of the mixing angles – $\theta_{12}, \theta_{13}, \theta_{23}$ – and one mass squared difference, Δ_{LSND} . In a realistic analysis one has to average the probabilities over the L/E distributions of various experiments and fold it with the detector cross-sections. We adopt the approach followed in [42] since one mass scale dominance is a good approximation in our case also. As noted in [42] in this limit one can make a one to one correspondence between $\sin^2 2\theta$ as obtained from a two flavour analysis and the angular factor appearing in a three generation calculation. If we now fix Δm^2 around $\Delta_{LSND} \sim 6 \text{ eV}^2$ then from the

bound on $\sin^2 2\theta$ at this Δm^2 from two flavour exclusion contours one can constrain the three generation mixings. While the other experiments present the exclusion contours at 90% C.L., LSND gives their plots at 95% C.L. [1]. Thus for this we use the quoted value for the probability at 90% C.L. and use the limit $\sin^2(\pi L/\lambda_{LSND}) \rightarrow 1$.

The probabilities in the atmospheric neutrino case are functions of the three mixing angles $\theta_{12}, \theta_{13}, \theta_{23}$ and one mass squared difference. In our analysis we approximate the $\sin^2(\pi L/\lambda_{ATM})$ factor by its averaged value 0.5 as is often done in the context of the sub-GeV data [48, 49, 50]. This can be improved by an averaging over the incident neutrino energy spectrum, the zenith-angle of the beam as well as the final lepton energy [48, 42]. r_{MC} is taken to be 0.45 from a detailed Monte-Carlo simulation including the effects of muon polarisation [51]. Using the sub-GeV Kamiokande results:

$$0.48 \leq R \leq 0.73 \text{ (90\%C.L.)} \quad (36)$$

We determine how much of the area, admissible from neutrino oscillation searches at laboratory, permits R to lie in the above range for fixed values of the third mixing angle. The allowed ranges of this mixing angle consistent with the atmospheric data are also obtained.

Finally we check the compatibility of the mixing angles found from this combined analysis with the solar neutrino results. The sensitivity of CHORUS and NOMAD in these areas are explored. Below we discuss the results for each mass spectrum.

Mass Spectrum (i)

The various constraints in this case from the accelerator and reactor results are:

$$2s_{13}^2 c_{13}^2 < 0.05 \quad (Bugey) \quad (37)$$

$$4s_{23}^2 c_{13}^2 (1 - c_{13}^2 s_{23}^2) < 0.08 \quad (CDHSW) \quad (38)$$

$$4s_{13}^2 c_{13}^2 s_{23}^2 < 0.003 \quad (E776) \quad (39)$$

$$0.0002 \leq 4s_{13}^2 c_{13}^2 s_{23}^2 \leq 0.0069 \quad (LSND) \quad (40)$$

$$4s_{23}^2 c_{23}^2 c_{13}^4 < 0.02 \quad (E531) \quad (41)$$

From the Bugey constraint (37)

$$s_{13}^2 \lesssim 0.026 \text{ or } s_{13}^2 \gtrsim 0.974.$$

Confining s_{13}^2 within these limits we scan the whole range $0 \leq s_{23}^2 \leq 1$ to determine the admitted area in the $s_{13}^2 - s_{23}^2$ plane consistent with the accelerator and reactor experiments listed above. A large portion of the parameter space can be ruled out combining all the restrictions and three allowed sectors are obtained – presented in figs. 2a, 2b and 2c respectively.

Fig. 2a shows the zone where $0.974 \lesssim s_{13}^2 < 1.0$. As is clear from the figure, the most stringent limit on s_{23}^2 , in this range, comes from E776 and LSND constraints. The permitted area of fig. 2a corresponds to the case $s_{13}^2 \rightarrow 1$. In this regime the relevant probabilities for atmospheric neutrinos given by eqns. (15) to (17) can be expressed as $P_{\nu_e \nu_e} \simeq 1$, $P_{\nu_e \nu_\mu} \simeq 0$, $P_{\nu_\mu \nu_\mu} \simeq 1 - \frac{1}{2} \sin^2(2\theta_{12} + 2\theta_{23})$. This is the $\nu_\mu - \nu_\tau$ oscillation limit, where consistent solutions to the atmospheric puzzle may be obtained. However for the solar neutrino survival probability, eqn. (23), the limit $s_{13}^2 \rightarrow 1$ would imply that the coefficient of the vital term responsible for the MSW effect, P_{MSW} , becomes very small. Consequently $P_{\nu_e \nu_e} \rightarrow 1$ due to the factor s_{13}^4 in eqn. (23) contrary to the results from the solar neutrino experiments discussed in section 2.3. Similarly for the vacuum oscillation probability (eqn. (18)) also one would require that the factor $c_{13}^4 c_{12}^4$ multiplying the energy and Δm^2 dependent term, P_{2VAC} should not be too small which would again prefer low s_{13}^2 . Thus this area is disfavoured by the solar neutrino data.

For low s_{13}^2 ($\lesssim 0.026$) the allowed values of s_{23}^2 is severely constrained by E531 result and only very high (> 0.99) or very low (< 0.01) s_{23}^2 are admissible.

Fig. 2b shows the low s_{13}^2 – high s_{23}^2 zone. In this regime E776 data puts a stronger constraint on s_{13}^2 than Bugey and sets the limit $s_{13}^2 < 0.001$. In this part of the parameter space a consistent solution to the atmospheric neutrino anomaly cannot be found. This region corresponds to $s_{13}^2 \rightarrow 0$, $s_{23}^2 \rightarrow 1$, whence from eqns. (15) to (17) $P_{\nu_e \nu_e} \simeq 1 - 2c_{12}^2 s_{12}^2$, $P_{\nu_e \nu_\mu} \simeq 0$ and $P_{\nu_\mu \nu_\mu} \simeq 1$. Thus in this zone $\nu_e - \nu_\tau$ oscillations take place driving the ratio of ratios R in a direction opposite to that required.

Fig. 2c is the low s_{13}^2 – low s_{23}^2 region. In this portion of the parameter space most severe restrictions are from E531, LSND and Bugey giving the following constraints: $0.01 < s_{13}^2 < 0.026$, $0.002 < s_{23}^2 < 0.005$. The angles in this sector can be approximated as $s_{13} \rightarrow 0$, $s_{23} \rightarrow 0$. In this limit the relevant probabilities for the atmospheric neutrinos (eqns. (15) to (17)) are $P_{\nu_e \nu_e} \simeq 1 - 2c_{12}^2 s_{12}^2$, $P_{\nu_e \nu_\mu} \simeq 2c_{12}^2 s_{12}^2$ and $P_{\nu_\mu \nu_\mu} \simeq 1 - 2c_{12}^2 s_{12}^2$. Thus this belongs approximately to the $\nu_e - \nu_\mu$ oscillation region where the atmospheric anomaly can be explained consistently. Varying s_{13}^2 and s_{23}^2 in the range shown in fig. 2c the limits on s_{12}^2 compatible with the atmospheric neutrino constraint (36) are presented in fig. 3. Two allowed bands are obtained for s_{12}^2 : $0.10 \lesssim s_{12}^2 \lesssim 0.37$ and $0.61 \lesssim s_{12}^2 \lesssim 0.88$. Taking six different s_{12}^2 s, from the above range corresponding to the edges of the two permitted zones and the parts inside them, the allowed area in the $s_{13}^2 - s_{23}^2$ plane from accelerator, reactor and atmospheric neutrino data is shown shaded in fig. 4. Compatibility with the solar neutrino data disfavours the high values of s_{12}^2 and only part of the parameter spaces shown in figs. 2c, 3 and 4 satisfy all the experimental constraints.

Fixing $\Delta_{LSND} \sim 6 \text{ eV}^2$, from eqn. (13) $P_{\nu_\mu \nu_\tau} = 0.16 s_{23}^2 c_{23}^2 c_{13}^4$ for CHORUS and NOMAD. For typical values of mixing angles from this combined allowed zone, namely, $s_{13}^2 = 0.003$ and $s_{23}^2 = 0.02$, $P_{\nu_\mu \nu_\tau} \sim 3.12 \times 10^{-3}$, which is greater than the minimum

sensitivity, 10^{-4} , of these experiments and can be marginally within their reach.

Mass Spectrum (ii)

In this case the constraints on mixing angles at $\Delta_{LSND} \sim 6 \text{ eV}^2$ from the various laboratory experiments are:

$$2c_{13}^2 c_{12}^2 - 2c_{13}^4 c_{12}^4 < 0.05 \quad (\text{Bugey}) \quad (42)$$

$$4c_{12}^2 s_{12}^2 < 0.08 \quad (\text{CDHSW}) \quad (43)$$

$$4c_{12}^2 s_{12}^2 c_{13}^2 < 0.003 \quad (\text{E776}) \quad (44)$$

$$0.0002 \leq 4c_{12}^2 s_{12}^2 c_{13}^2 \leq 0.0069 \quad (\text{LSND}) \quad (45)$$

$$4c_{12}^2 s_{12}^2 s_{13}^2 < 0.02 \quad (\text{E531, from } \nu_\mu \rightarrow \nu_\tau) \quad (46)$$

For this case also three allowed areas in the relevant $s_{12}^2 - s_{13}^2$ plane are obtained, from the laboratory constraints. The experiments which are most restrictive in this case can be different in general from the mass spectrum (i). These regions are displayed in figs. 5a, b and c respectively. The CDHSW constraint (43) gives,

$$s_{12}^2 \lesssim 0.02 \text{ or } s_{12}^2 \gtrsim 0.98.$$

Fig. 5a shows the area for which $s_{12}^2 \gtrsim 0.98$. Allowed ranges of s_{13}^2 in this region are determined by E776 and LSND. This corresponds to $s_{12}^2 \rightarrow 1$. In this limit for the atmospheric neutrinos $P_{\nu_e \nu_\mu} \simeq 0$ and $P_{\nu_\mu \nu_\mu} \simeq 1$, from the expressions (32) and (33). Thus this is the $\nu_e - \nu_\tau$ oscillation regime and is not consistent with the atmospheric anomaly.

For $s_{12}^2 \lesssim 0.02$, the Bugey constraint (42) restricts the permissible values of s_{13}^2 to be $\gtrsim 0.97$ or $\lesssim 0.03$.

Fig. 5b contains the area where $s_{12}^2 \lesssim 0.02$ and $s_{13}^2 \gtrsim 0.97$. In this region $s_{13}^2 \rightarrow 1$, $s_{12}^2 \rightarrow 0$. Then, the probabilities given by eqns. (31) to (33) for the atmospheric neutrinos assume the following forms: $P_{\nu_e \nu_e} \simeq 1 - 2c_{23}^2 s_{23}^2$, $P_{\nu_e \nu_\mu} \simeq 2c_{23}^2 s_{23}^2$ and $P_{\nu_\mu \nu_\mu} \simeq 1 - 2c_{23}^2 s_{23}^2$. Thus, in this limit $P_{\nu_\mu \nu_\tau} \simeq 0$ and the atmospheric puzzle can be explained by $\nu_e - \nu_\mu$ transitions. However, since $s_{13}^2 \rightarrow 1$, this region is incompatible with the solar neutrino flux measurements as is evident from (34) and (35).

Fig. 5c shows the area $0 < s_{12}^2 < 8 \times 10^{-4}$ and $0 < s_{13}^2 < 0.03$. Here, E776 data puts a tighter bound on s_{12}^2 than CDHSW. The constraint on s_{13}^2 is determined by Bugey. This region corresponds to the limit $s_{13}^2 \rightarrow 0$, $s_{12}^2 \rightarrow 0$. In this range eqns. (31) to (33) for atmospheric neutrinos imply $P_{\nu_e \nu_e} \simeq 1$, $P_{\nu_e \nu_\mu} \simeq 0$ and $P_{\nu_\mu \nu_\mu} \simeq 1 - 2c_{23}^2 s_{23}^2$. So this corresponds to $\nu_\mu - \nu_\tau$ oscillations in the atmosphere. Substituting these in (36) one gets the limits on s_{23}^2 as $0.162 < s_{23}^2 < 0.838$. A similar situation was discussed in [47], which considered the three generation limit of the mixing matrix (26). As in [47] for all s_{23}^2 lying within this limit the whole of the parameter space shown in fig. 5c

is consistent with the condition (36). Thus in fig. 6 we present the allowed region in the $s_{12}^2 - s_{13}^2$ plane consistent with accelerator, reactor and atmospheric neutrino data choosing one representative value of $s_{23}^2 (= 0.2)$ from the above range. The difference with [47] is, here, E776 constraints further narrows down the allowed range of s_{12}^2 . Since in this zone both s_{12}^2 and s_{13}^2 stay close to zero this is consistent with the solar neutrino results.

For CHORUS and NOMAD from eqn. (30) $P_{\nu_\mu\nu_\tau} = 0.16s_{12}^2c_{12}^2s_{13}^2$. Taking two typical values of s_{12}^2 and s_{13}^2 , namely, $s_{12}^2 = 10^{-4}$ and $s_{13}^2 = 0.02$, from the combined allowed zone, $P_{\nu_\mu\nu_\tau} \sim 10^{-6}$ which is below the minimum sensitivity attainable in these experiments.

We observe that in both cases, the solar neutrino survival probabilities eqns.(18) and (34) for the vacuum oscillation case and eqns. (23) and (35) for matter oscillations depend on Δ_{14}, θ_{14} as well as on combinations of $\theta_{12}, \theta_{13}, \theta_{23}$ which depend on the mass pattern. Fixing the values of these mixing angles in the region determined by the atmospheric and laboratory results one can find the allowed area in the $\Delta_{14} - \sin^2 2\theta_{14}$ plane using the solar neutrino data. The solar neutrino probabilities in this case differ from the two generation $\nu_e - \nu_s$ oscillations case, due to the presence of the mixing angles with the other generations. Also, in the two generation case involving just ν_e and ν_s Kamiokande would be sensitive to ν_e s only but here one has the additional possibility of a simultaneous transition to ν_μ s as well as ν_τ s which can interact in the Kamiokande detector by virtue of their neutral current interactions. It has been shown in [41, 42] that the appearance of one mixing angle in the expression of probability leads to a larger area in the MSW parameter space. Similar conclusions might be obtained here also. The following points of differences are to be noted:

- (i) In [41] or [42] three generations are involved and the resonance condition as well as the survival probabilities are affected by the presence of only one additional mixing angle, whereas here one has two or three such mixings.
- (ii) In the above references oscillation between active species were considered and hence the term involving the neutron density was absent and the jump-probability retained its two generation form. Here due to the asymmetric interaction between the active and the sterile species the jump-probability between the first and the fourth state is also affected by mixing with the other generations.

A definitive prediction regarding how these would change the two flavour allowed zones need a detailed numerical analysis of the solar neutrino data including the neutrino fluxes, density profile, interaction cross-sections and a thorough treatment of the theory errors and their correlations. This is not performed here.

Similarly in the vacuum oscillation case also one can probe whether the presence of the other mixing angles will alter the two flavour parameter space.

We note that for the mass spectrum (ii) in the combined allowed zone depicted in fig. 6, both s_{12}^2 and s_{13}^2 stay close to 0. Thus in this case, from eqns. (34) and (35) for the vacuum and matter oscillation case respectively, the presence of the other

mixing angles is not expected to change the two flavour parameter space significantly.

6 Summary and Conclusions

We have performed a combined analysis of the accelerator, reactor, atmospheric and solar neutrino data in a four generation framework introducing a sterile neutrino, ν_s . In such a scenario there are in general six mass squared differences, three of which are independent and six mixing angles, neglecting CP violation in the lepton sector. We assume that ν_s mixes only with ν_e , thus reducing the number of mixing angles to four – $\theta_{12}, \theta_{13}, \theta_{23}$ and θ_{14} . Fixing the three independent Δm^2 s around the ranges from two generation analyses of the LSND, atmospheric and solar neutrino data, we determine the mixing angles consistent with all the experimental constraints. We consider a picture where Δ_{14} is fixed in the solar neutrino range (either MSW or vacuum oscillation). Then one can think of two different mass patterns for the remaining five Δm^2 s – the mass spectrum (i) in which two Δm^2 s are in the atmospheric range and the other three in the LSND range and the mass spectrum (ii) where one Δm^2 is in the atmospheric range and the remaining four in the LSND range. For both cases one can parametrise the mixing matrix in such a way that the probabilities for the accelerator and reactor experiments are functions of only two mixing angles and one independent Δm^2 viz Δ_{LSND} . Fixing Δ_{LSND} at $6eV^2$ we map out the allowed zone in the $\sin^2 \theta_{13} - \sin^2 \theta_{23}$ ($\sin^2 \theta_{12} - \sin^2 \theta_{13}$) plane for the mass spectrum (i) ((ii)). Using the atmospheric neutrino constraint the above area can be further restricted and the permissible ranges for the remaining mixing angle can be determined. Next we examine whether the combined allowed area thus obtained is compatible with the solar neutrino results.

In general for both mass patterns the following picture emerges: the accelerator and reactor experiments give three allowed sectors of relevant mixing angles. In two of these zones a simultaneous solution to the atmospheric anomaly is possible. One among these is disfavoured by the solar neutrino data – leaving us with a narrow range for permitted θ_{12}, θ_{13} and θ_{23} . For the mass spectrum (i) the admitted zone from all the input information is the one where the atmospheric puzzle can be explained by $\nu_e - \nu_\mu$ oscillation, while for the mass spectrum (ii) in the combined allowed zone it is due to $\nu_\mu - \nu_\tau$ oscillations. For both mass patterns $P_{\nu_\mu \nu_\tau}$ for CHORUS and NOMAD is much below the minimum reach of these experiments in the region where the solution to the atmospheric problem is via $\nu_\mu - \nu_\tau$ oscillations. For mass spectrum (ii) this being the combined allowed zone, cannot be explored by CHORUS and NOMAD whereas for (i) in the favoured zone $P_{\nu_\mu \nu_\tau}$ for CHORUS and NOMAD can be greater than the minimum sensitivity of 10^{-4} and could be probed by these experiments.

In conclusion we would like to mention that though a three flavour mixing scheme cannot accommodate the three hierarchically different mass ranges required for LSND, atmospheric and solar neutrino oscillations, in a four generation framework with an

additional sterile neutrino there are more than one possible mass spectrums that can account for all the data simultaneously. We discussed two such mass spectrums. In both cases our analysis assumes that the solar neutrino oscillation is driven mainly by $\nu_e - \nu_s$ transitions. If this scenario is confirmed by the future solar neutrino experiments and the other experimental inputs do not change significantly as more data accumulates then it is necessary to go to a four generation picture. We have shown that the implications of CHORUS and NOMAD are different in the two cases and thus they can distinguish between these.

In this article the allowed areas are obtained by fixing $\Delta_{LSND} \sim 6 \text{ eV}^2$. LSND is sensitive to the range 1-10 eV^2 and it remains to be seen what best-fit value, consistent with KARMEN and BNL-E776, emerges when more data is accrued. We believe that the general conclusions obtained in this analysis will remain the same for any other value of Δm^2 in the above range, though the precise values of the allowed mixing angles may be different.

The author is indebted to Dr. Amitava Raychaudhuri for many useful suggestions, discussions, a careful scrutiny of the manuscript and encouragement at every stage of this work. She also wishes to thank Dr. Kamales Kar for discussions, help and encouragement. Financial support from the Council of Scientific and Industrial Research, India is acknowledged.

Table 1: The characteristics of the most restrictive accelerator and reactor experiments. λ_{LSND} and λ_{ATM} are calculated for $\Delta_{LSND} \sim 6 \text{ eV}^2$ and $\Delta_{ATM} \sim 10^{-2} \text{ eV}^2$ respectively.

Experiment	E	L	λ_{LSND}	λ_{ATM}
Bugey	$\sim 5 \text{ MeV}$	$\sim 40 \text{ m}$	$\sim 2.08 \text{ m}$	1250 m
CDHSW	$2 < E < 20 \text{ GeV}$	$\sim 1 \text{ km}$	$(0.83 - 8.33) \text{ km}$	$(500 - 5000) \text{ km}$
E776	$1 - 10 \text{ GeV}$	$\sim 1 \text{ km}$	$(0.416 - 4.16) \text{ km}$	$(250 - 2500) \text{ km}$
E531	$\sim 50 \text{ GeV}$	0.949 km	$\sim 22 \text{ km}$	$\sim 12500 \text{ km}$
LSND	$(36 - 60) \text{ MeV}$	30 m	$(15 - 25) \text{ m}$	$(9 - 15) \text{ km}$
CHORUS/NOMAD	30 GeV	0.8 km	12.5 km	7500 km

FIGURE CAPTIONS

Figure 1: The level diagrams showing the possible mass hierarchies (not to scale).

Figure 2: The allowed region in the $s_{13}^2 - s_{23}^2$ plane from accelerator and reactor data for the mass pattern (i)

(a) The region between the solid lines is allowed by LSND; the area to the right of the big-dashed line is permitted by E776 and that below the small-dashed line is allowed from CDHSW.

(b) The admitted area from LSND is between the solid lines while that from CDHSW and E-531 is above the small-dashed and medium-dashed lines respectively. The area to the left of the big-dashed line is allowed from E776.

(c) The area between the solid lines is allowed by LSND while that below the big-dashed, small-dashed and medium-dashed lines are allowed from E776, CDHSW and E531 respectively.

In each of these the combined allowed area is marked ‘allowed’.

Figure. 3: The allowed region in the $s_{12}^2 - s_{23}^2$ plane consistent with accelerator, reactor and atmospheric neutrino constraints. s_{13}^2 is varied in the range determined from fig. 2(c).

Figure 4: The allowed area of fig. 2c that is consistent with the atmospheric neutrino constraint is shown shaded for six different values of s_{12}^2 from the admitted range in fig. 3.

Figure 5: The allowed region in the $s_{12}^2 - s_{13}^2$ plane from accelerator and reactor data for the mass pattern (ii)

(a) The area between the curved solid lines is allowed by LSND, while that to the right of the vertical solid line is consistent with the CDHSW constraint; the zones above the small-dashed, medium-dashed and big-dashed lines are allowed from Bugey, E531 and E776 respectively.

(b) The permissible area from LSND is between the curved solid lines; the areas above the small-dashed, medium-dashed and big-dashed lines are allowed from Bugey, E531 and E776 respectively; the region to the left of the vertical solid line is admitted from CDHSW.

In each of these figures the area marked as ‘allowed ’ is consistent with all the constraints.

Figure 6: The allowed region of fig. 5c that is consistent with the atmospheric neutrino constraint is shown shaded.

References

- [1] C. Athanassopoulos *et al.*, nucl-ex/9504002 (1995); W.C. Louis, Nucl. Phys. (Proc. Suppl.) **B38**, 229 (1995).
- [2] J.R. Primack *et al.*, Phys. Rev. Lett. **74**, 2160 (1995).
- [3] G. Raffelt and J. Silk, hep-th/9502306.
- [4] See for example G.M. Fuller, J.R. Primack and Y.Z. Qian, astro-ph/9502081; D.O. Caldwell and R.N. Mohapatra, Preprint No. UCSB-HEP-95-1, hep-ph/9503316; S.M. Bilenky *et al.*, Preprint No. DFTT 25/95, JHU-TIPAC 95013, hep-ph 9504405 (1995).
- [5] J. N. Bahcall and M. H. Pinsonneault, Rev. Mod. Phys. **64**, 885 (1992); S. Turck-Chièze and I. Lopes, Astrophys. J. **408**, 347 (1993); See also J. N. Bahcall and M. H. Pinsonneault, Preprint No. IASSNS-AST 95/24, to appear in Rev. Mod. Phys. October 1995.
- [6] N. Hata and P. Langacker, Phys. Rev. **D47**, 2220 (1993); J.N. Bahcall, Phys. Lett. **B338**, 276 (1994); W. Kwong and S.P. Rosen, Phys. Rev. Lett. **73**, 369 (1994); S. Parke, Phys. Rev. Lett. **74**, 839 (1994).
- [7] For a review on vacuum oscillation see S.M. Bilenky and B.M. Pontecorvo, Sov. Phys. Usp. **20**, 776 (1977).
- [8] L. Wolfenstein Phys. Rev. **D34**, 969 (1986); S. P. Mikheyev and A. Yu. Smirnov, Sov. J. Nucl Phys. **42(6)** 913 (1985); Nuovo Cimento **9c** 17 (1986).
- [9] N. Hata and P. Langacker, Phys. Rev. **D50**, 632 (1994)
- [10] X. Shi, D. Schramm and B. Fields, Phys. Rev. **D48**, 2563 (1993).
- [11] N. Hata, Univ. of Pennsylvania Preprint No. UPR-0605T, 1994.
- [12] P.I. Krastev and S.T. Petcov, Phys. Rev. Lett. **72**, 1960 (1994).
- [13] K. S. Hirata *et al.*, Phys. Lett. **B280**, 146 (1992).
- [14] Y. Fukuda *et al.*, Phys. Lett. **B335**, 237 (1994).
- [15] D. Casper *et al.*, Phys. Rev. Lett. **66**, 2561 (1991); R. Becker-Szendy *et al.*, Phys. Rev. **D46**, 3720 (1992).
- [16] Ch. Berger *et al.*, Phys. Lett. **B227**, 489 (1989).
- [17] M. Agiletta *et al.*, Europhys. Lett. **8**, 611 (1989).

- [18] M. Goodman *et al.*, Nucl. Phys. (Proc. Suppl.) **B38**, 337 (1995).
- [19] The usage of the ‘ratio of ratios’ R as a valid indicator of the neutrino anomaly has been recently critically examined. see G.L. Fogli and E. Lisi, Institute for Advanced Study report IASSNS-AST 95/21.
- [20] H. Minakata, Preprint No. TMUP-HEL-9502, March 15, 1995; Preprint No. TMUP-HEL-9503, hep-ph/9504222, (1995).
- [21] L. Bento and J.W.F. Valle, Phys. Lett. **B264**, 373 (1991); J. Peltoniemi, A.Yu. Smirnov and J.W.F. Valle, Phys. Lett. **B286**, 321 (1992); J. Peltoniemi *et al.*, Phys. Lett. **B298**, 383 (1993); D.O. Caldwell and R.N. Mohapatra, Phys. Rev. **D48**, 3259 (1993).
- [22] See for example E. Ma and J. Pantaleone, Preprint No. UCRHEP-T140, March (1995); E. Ma and P. Roy, Preprint No. UCRHEP-T145, TIFR/TH/95-17 April (1995), E. J. Chun, Anjan S. Joshipura and A. Yu. Smirnov, Report-no: IC/95/76, PRL-TH/95-7, hep-ph/9505275 (1995).
- [23] For a review see L. Oberauer and F. Von. Feilitzsch, Rep. Prog. Phys. **55**, 1093 (1992).
- [24] B. Achkar *et al.*, Nucl. Phys. **B434**, 503 (1995).
- [25] F. Dydak *et al.*, Phys. Lett. **B314**, 281 (1984).
- [26] B. Armbruster *et al.*, Nucl. Phys. (Proc. Suppl.) **B38**, 235 (1995).
- [27] L. Borodovsky *et al.*, Phys. Rev. Lett. **68**, 274 (1992).
- [28] N. Ushida *et al.*, Phys. Rev. Lett. **57**, 2898 (1986).
- [29] M. de Jong *et al.*, CERN-PPE/93-131 (1993); N. Armenise *et al.*, CERN-SPSC/90-42 (1990).
- [30] P. Astier *et al.*, CERN-SPSLC/91-21, CERN-SPSLC/91-48, CERN-SPSLC/P261 Add.1 (1991).
- [31] D. Saltzberg, hep-ph-9504343.
- [32] B.T. Cleveland *et al.*, Nucl. Phys. (Proc. Suppl.) **B38**, 47 (1995).
- [33] The theoretical rates quoted are from the last one in ref. [5], which is the latest in the series.
- [34] P. Anselman *et al.*, Phys. Lett. **B285**, 376 (1992); **B327**, 377 (1994).

- [35] A.I. Abazov *et. al.*, Phys. Rev. Lett. **67**, 3332 (1991); G. Nico *et. al.*, in Proc. of the XXVII Int. Conf. on High Energy Physics (Glasgow), Eds. P.J. Bussey and I.G Knowles, Inst. of Phys. Publising, Bristol, p965 (1995);
- [36] K.S. Hirata *et. al.*, Phys. Rev **D44**, 2241 (1991); Y. Suzuki *et. al.*, Nucl. Phys. (Proc. Suppl.) **B38**, 54 (1995).
- [37] G.T. Ewan *et. al.*, Sudbury Neutrino Observatory proposal, Pub. No. SNO-87-12 (1987); Y. Totsuka, Tokyo Univ. Preprint No. ICRR-227-90-20 (1990), C. Arpellsa *et.al.*, Borexino Proposal, Eds. G. Bellini *et. al.*, Univ. of. Milano (1991).
- [38] M. Kobayashi and K. Maskawa, Progr. Theor. Phys. **49** 652 (1973); L. Maiani, Phys. Lett. **B62**, 183 (1976); U. Turke, *et. al.*, Nucl. Phys. **B258**, 313 (1985); H. Harari and M. Leurer, Phys. Lett. **B 181**, 123 (1986).
- [39] E.D. Carlson, Phys. Rev. **D34**, 1454 (1986).
- [40] T.K. Kuo and J. Pantaleone, Rev. Mod. Phys. **61**, 937 (1989) and references therein; See also D. Harley, T.K. Kuo and J. Pantaleone, Phys. Rev. **D47**, 4059 (1993); M. Narayan *et. al.*, Preprint No. IMSc/95-96/001 (1995).
- [41] A.S. Joshipura and P.I. Krastev, Phys. Rev. **D50**, 3484 (1994).
- [42] G.L. Fogli, E. Lisi and D. Montanio, Phys. Rev. **D49**, 3626 (1994).
- [43] V. Barger *et al.*, Phys. Rev **D43**, 1110 (1991); Phys. Rev. Lett. **65**, 3084 (1990); **69**, 3135 (1992); A. Acker, S. Pakvasa and J. Pantaleone, Phys. Rev. **D43**, 1754 (1991); P.I. Krastev and S.T. Petcov, Phys. Lett. **B285**, 85 (1992); **299**, 99 (1993).
- [44] V. Barger *et. al.*, Phys. Rev. **D43**, R1759 (1991).
- [45] V. Barger, *et. al.*, Phys. Lett. **B93**, 195 (1980); J. Phys. G **6**, L165 (1980); V. Barger, K. Whisnant and R.J.N. Phillips, Phys. Rev **D22**, 1636 (1980); A. De Rujula *et. al.*, Nucl. Phys.**B168**, 54 (1980).
- [46] J.J. Gomez-Cadenas and M.C. Gonzalez-Garcia, Preprint No. CERN-TH/95-80, April (1995).
- [47] S. Goswami, K. Kar and A. Raychaudhuri, Preprint No. CUPP/95-3, hep-ph/9505395 (1995).
- [48] V. Barger and K. Whisnant, Phys. Lett. **B209**, 365 (1988).
- [49] A. Acker, J.G. Learned, S. Pakvasa and T.J. Weiler, Phys. Lett. **B298**, 149 (1993).
- [50] A. Acker, A.B. Balantekin and F. Loreti, Preprint No. Mad/NT/93-07, MAD/PH/# 774, July (1993).

- [51] G. Barr, T.K. Gaisser and T. Stanev, Phys. Rev **D39** 3532 (1989); T.K. Gaisser, T. Stanev and G. Barr, *ibid* **D38**, 85 (1988).

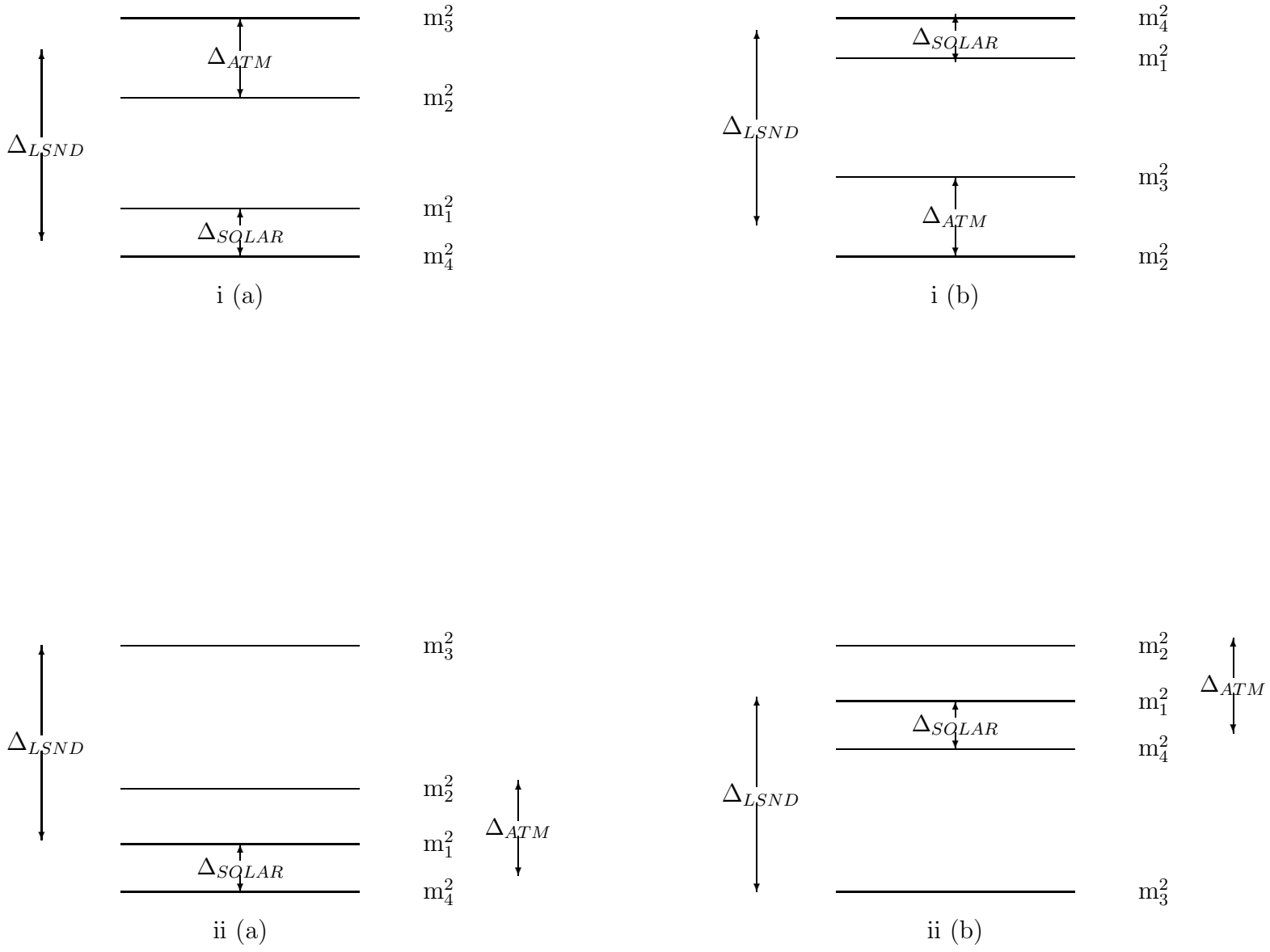


Fig. 1